Electron interference in mesoscopic devices in the presence of nonclassical electromagnetic fields

D. I. Tsomokos[1,2], C. C. Chong[3], A. Vourdas[1]

[1]Department of Computing, University of Bradford, Bradford, BD7 1DP, England
[2]Department of Physics, Astrophysics and Mathematics, University of Hertfordshire, Hatfield, AL10 9AB, England
[3]Institute of High Performance Computing, 1 Science Park Road, 117528, Singapore

Abstract. The interaction of mesoscopic interference devices with nonclassical electromagnetic fields is studied. The external quantum fields induce a phase factor on the electric charges. This phase factor, which is a generalization of the standard Aharonov-Bohm phase factor, is in the case of nonclassical electromagnetic fields a quantum mechanical operator. Its expectation value depends on the density matrix describing the nonclassical photons and determines the interference. Several examples are discussed, which show that the quantum noise of the nonclassical photons destroys slightly the electron interference fringes. An interesting application arises in the context of distant electron interference devices, irradiated with entangled photons. In this case the interfering electrons in the two devices become entangled. The same ideas are applied in the context of SQUID rings irradiated with nonclassical electromagnetic fields. It is shown that the statistics of the Cooper pairs tunneling through the Josephson junction depend on the statistics of the photons.

PACS numbers: 42.50.Dv, 42.50.Lc, 03.65.Vf, 03.65.Ud

1. Introduction

Interference of electrons in the presence of a magnetostatic flux has been studied for a long time since the work of Aharonov and Bohm [1]. The Aharonov-Bohm phase factor is acquired by electric charges that encircle a magnetic flux, even if the flux vanishes in the vicinity of the paths of the charges. The effect has inspired numerous applications in solid state physics [2]. In particular we mention extensive theoretical and experimental research on persistent currents in mesoscopic rings [3, 4, 5, 6, 7, 8].

Electron interference in the presence of a time-dependent magnetic flux (i.e., electromagnetic fields) has also been studied [9, 10, 11, 12, 13, 14]. The intention here is not to prove the reality of the vector potential, but to study how electromagnetic fields affect interfering electrons.

The next step in this line of research is to consider nonclassical electromagnetic fields [15, 16] which are carefully prepared in a particular quantum state, and study their effect on quantum interference [9, 10]. In this case it is shown that the quantum noise in the electromagnetic field destroys partly the electron interference fringes. Different types of nonclassical electromagnetic fields are characterized by different quantum statistics; and we will show explicitly that the electron interference results depend on the photon statistics.

An important feature of multimode quantum electromagnetic fields is entanglement. Two electromagnetic field modes can be factorizable (uncorrelated); or separable (classically correlated); or entangled (quantum mechanically correlated) [17]. Entangled electromagnetic fields have been produced experimentally in laboratories for a long time [18]. In the context of this review article, we consider two distant mesoscopic electron interference devices that are irradiated with a two-mode nonclassical electromagnetic field [19]. Each field mode is coupled to one of the mesoscopic devices. For entangled electromagnetic fields, the electric currents in the distant mesoscopic devices become correlated. Moreover the induced correlations of the electrons depend on the nature of the correlation between the external photons.

Similar phenomena can be studied in the context of superconducting quantum interference devices (SQUID) [20, 21, 22, 23]. Experimental work has so far concentrated on the interaction of mesoscopic devices with classical electromagnetic fields. However the interaction of a Josephson device with a single microwave photon has recently been studied experimentally in reference [24].

The interaction of mesoscopic SQUID rings with nonclassical electromagnetic fields has been studied theoretically in [25, 26, 27, 28]. In this case the Josephson current is a quantum mechanical operator, whose expectation value with respect to the density matrix of the external photons, yields the observed current. The interaction of entangled electromagnetic fields with two spatially separated SQUID rings has been studied in [29, 30]. It has been shown that the photon correlations can be transferred to the Cooper pair currents measured in the two distant SQUID rings.

In this interdisciplinary work we bridge the gap between electron coherence

in mesoscopic physics and nonclassical phenomena in quantum optics. Work on entanglement of several mesoscopic devices has been reported in [31].

The paper is organized as follows. In section 2 we describe certain one-mode and two-mode nonclassical fields, which are relevant to the rest of our work, and derive the corresponding Weyl function [32]. In section 3 we discuss the magnetic flux and the electromotive force operators, which are the dual quantum variables in our context.

We subsequently turn our attention to electron interference phenomena. In section 4 we describe the standard Aharonov-Bohm phase factor in electron interference that is induced by a magnetostatic flux. In section 5 we describe the electron phase factor operator that is induced by nonclassical electromagnetic fields [9]. It is explained that the expectation value of the phase factor and, consequently, of the electron intensity distribution depend on the quantum state of the external photons.

We stress that accurate knowledge of the quantum state of the electromagnetic field enables us to calculate not only the average intensity of the interfering electrons, but also their full statistics (higher order correlations). In section 6 we quantify the quantum statistics of the interfering electrons using the autocorrelation function and its Fourier transform, the spectral density. It is shown that the quantum statistics of the interfering electrons depend on the quantum statistics of the photons [10]. In section 7 we describe how two spatially separated electron interference experiments, which interact with entangled fields, become correlated [19].

In section 8 we study the interaction of nonclassical electromagnetic fields with mesoscopic SQUID rings. In the case of two distant SQUID rings, which are coupled to two entangled electromagnetic fields, we show that the quantum currents tunneling through the distant Josephson junctions become entangled [29]. We conclude with a summary of the results in section 9.

2. Nonclassical electromagnetic fields

In this section we introduce the nonclassical states of the electromagnetic field that are relevant to the rest of our work. We define the Weyl function and provide its value in the case of number, coherent, squeezed, and thermal states. It is noted that we use theoretical units, in which $k_{\rm B} = \hbar = c = 1$.

2.1. One-mode quantum states of the electromagnetic field

Nonclassical electromagnetic fields are carefully prepared in a particular quantum state and are described by a density matrix ρ. In this case we know the average values $\langle E\rangle, \langle B\rangle$ of the electric and magnetic fields, the standard deviations $\Delta E, \Delta B$ and also their higher moments. Another quantity which describes the fields is the photon counting distribution function

$$P(N) \equiv \langle N|\rho|N\rangle. \tag{1}$$

Various examples of nonclassical electromagnetic fields are given below.

2.1.1. Number states The number states $|N\rangle$ are defined as:

$$|N\rangle = \frac{(\hat{a}^\dagger)^N}{\sqrt{N!}}|0\rangle. \tag{2}$$

2.1.2. Coherent states The coherent states $|A\rangle$ are defined as:

$$|A\rangle = D(A)|0\rangle \tag{3}$$

where $D(A)$ is the displacement operator

$$D(z) = \exp(z\hat{a}^\dagger - z^*\hat{a}). \tag{4}$$

The photon counting distribution is in this case Poissonian.

2.1.3. Squeezed states The squeezing operator is defined as

$$S(r\varphi) = \exp\left[-\frac{r}{4}\exp(-i\varphi)\hat{a}^{\dagger 2} + \frac{r}{4}\exp(i\varphi)\hat{a}^2\right] \tag{5}$$

where the r, φ are real numbers and r is known as the squeezing parameter. Squeezed states $|A; r\varphi\rangle$ are defined by acting on the coherent state $|A\rangle$, with the squeezing operator

$$|A; r\varphi\rangle = S(r\varphi)|A\rangle = S(r\varphi)D(A)|0\rangle. \tag{6}$$

In this case $P(N)$ can be sub-Poissonian. The average number of photons is

$$\langle N\rangle_{\rm sq} = \left[\sinh\left(\frac{r}{2}\right)\right]^2 + \left[\cosh\left(\frac{r}{2}\right) - \sinh\left(\frac{r}{2}\right)\right]^2 |A|^2. \tag{7}$$

In figure 1 we have plotted the electric field as a function of time in the case of coherent and squeezed light. Both the average value $\langle\hat{E}\rangle$ and the quantum noise $\Delta\hat{E}$ are shown. The parameters are chosen so that the average value of the electric field is the same in both examples. It is seen that the two fields differ in the quantum noise $\Delta\hat{E}$. The anti-bunching of photons in squeezed states, in comparison to the Poissonian statistics in the case of coherent states, is also shown in the figure. These two types of nonclassical electromagnetic fields will be used later, in the context of electron interference (i.e., we will study the situation where these nonclassical electromagnetic fields are coupled with electron interference devices). It will be shown there that they produce different results for the electron interference.

2.1.4. Thermal states The thermal states are defined through the density matrix

$$\begin{aligned}\rho_{\rm th} &= [1 - \exp(-\beta\omega)]\exp(-\beta\omega\hat{a}^\dagger\hat{a}) \\ &= [1 - \exp(-\beta\omega)]\sum_{n=0}^{\infty}\exp(-\beta\omega n)|n\rangle\langle n|\end{aligned} \tag{8}$$

where β is the inverse temperature. In this case the average number of photons is

$$\langle N\rangle_{\rm th} = \frac{1}{\exp(\beta\omega) - 1}. \tag{9}$$

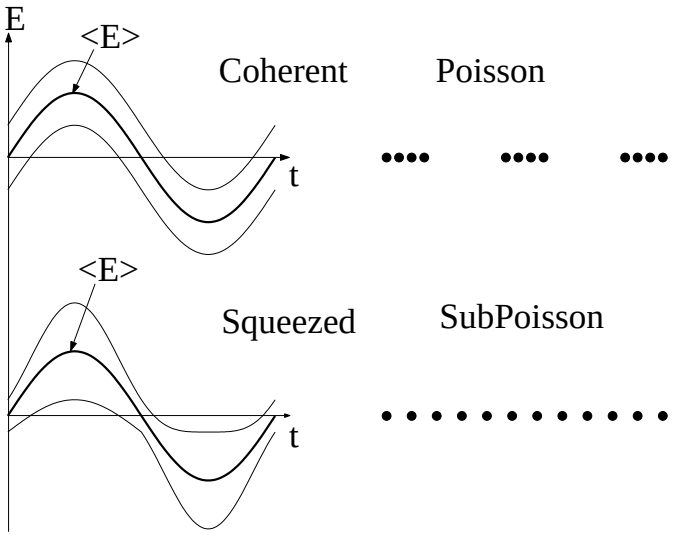

Figure 1. The electric field of coherent and squeezed light as a function of time. Both the average value $\langle \hat{E} \rangle$ and the quantum noise $\Delta \hat{E}$ are shown. The anti-bunching of photons in squeezed states, in comparison to the Poissonian statistics in coherent states, is also shown.

2.2. Weyl functions

The Wigner and Weyl (or characteristic) functions play an important role in quantum mechanics [32]. The Weyl function that corresponds to a quantum state described by a density operator ρ is defined in terms of the displacement operator of equation (4) as

$$\tilde{W}(z) \equiv \mathrm{Tr}[\rho D(z)]. \tag{10}$$

The tilde in the notation reflects the fact that the Weyl function $\tilde{W}$ is the two-dimensional Fourier transform of the Wigner function W. The $\tilde{W}(z)$ is a complex function, in general, whose absolute value obeys

$$0 \leq |\tilde{W}(z)| \leq 1. \tag{11}$$

For later use we give the Weyl function for various states. We start with the following relation [33]

$$\langle M|D(z)|N\rangle = \left(\frac{N!}{M!}\right)^{1/2} z^{M-N} \exp\left(-\frac{|z|^2}{2}\right) L_N^{M-N}(|z|^2) \tag{12}$$

where the L_k^α are Laguerre polynomials [34]. Therefore the Weyl function for a number state $|N\rangle$ is

$$\tilde{W}_{\mathrm{num}}(z) = \exp\left(-\frac{|z|^2}{2}\right) L_N(|z|^2). \tag{13}$$

The Weyl function for a coherent state $|A\rangle$ is

$$\tilde{W}_{\mathrm{coh}}(z) = \exp\left[-\frac{|z|^2}{2} + i2|Az|\sin(\arg z - \arg A)\right]. \tag{14}$$

The Weyl function for a squeezed state $|A; r\varphi\rangle$ is

$$\tilde{W}_{\rm sq}(z) = \exp(-Y + iX), \tag{15}$$
$$X = 2|Az| \left[\cosh\left(\frac{r}{2}\right)\sin(\arg z - \arg A) - \sinh\left(\frac{r}{2}\right)\sin(\arg z + \arg A + \varphi)\right],$$
$$Y = \frac{|z|^2}{2}\left[\cosh(r) + \sinh(r)\cos(2\arg z + \varphi)\right].$$

Finally for thermal states we have

$$\tilde{W}_{\rm th}(z = \zeta e^{i\omega t}) = \exp\left[-\frac{\zeta^2}{2}\coth\left(\frac{\beta\omega}{2}\right)\right], \tag{16}$$

where ζ is a real number. These relations have been given in reference [25].

2.3. Two-mode quantum states: separability versus entanglement

Nonclassical electromagnetic fields with several modes allow for correlations between the distinct field modes. The nature of the correlation can be classical or quantum [17].

Let ρ be the density matrix that describes a two-mode nonclassical electromagnetic field. Then the density matrices of the two fields are

$$\rho_{\rm A} \equiv {\rm Tr}_{\rm B}(\rho), \qquad \rho_{\rm B} \equiv {\rm Tr}_{\rm A}(\rho). \tag{17}$$

The density matrix ρ for the two-mode electromagnetic field state is factorizable if $\rho_{\rm fact} = \rho_{\rm A} \otimes \rho_{\rm B}$. The density matrix ρ is separable if

$$\rho_{\rm sep} = \sum_k P_k \rho_{{\rm A},k} \otimes \rho_{{\rm B},k} \tag{18}$$

where P_k are probabilities. In all other cases the density matrix $\rho_{\rm ent}$ is entangled.

2.3.1. Two-mode number states For later use we consider the (mixed) separable density operator

$$\rho_{\rm sep} = \frac{1}{2}(|N_1N_2\rangle\langle N_1N_2| + |N_2N_1\rangle\langle N_2N_1|). \tag{19}$$

We also consider the (pure) entangled state $|s\rangle = 2^{-1/2}(|N_1N_2\rangle + |N_2N_1\rangle)$, for example. The corresponding density operator is

$$\rho_{\rm ent} = \rho_{\rm sep} + \frac{1}{2}(|N_1N_2\rangle\langle N_2N_1| + |N_2N_1\rangle\langle N_1N_2|). \tag{20}$$

Clearly in this example the $\rho_{\rm sep}$ and the $\rho_{\rm ent}$ differ only in the above nondiagonal elements. In both the separable and the entangled case the reduced density operators of equation (17) are given by

$$\rho_{\rm sep,A} = \rho_{\rm ent,A} = \rho_{\rm sep,B} = \rho_{\rm ent,B} = \frac{1}{2}(|N_1\rangle\langle N_1| + |N_2\rangle\langle N_2|). \tag{21}$$

2.3.2. Two-mode coherent states We consider the two-mode coherent states in the classically correlated state

$$\rho_{\rm sep} = \frac{1}{2}(|A_1A_2\rangle\langle A_1A_2| + |A_2A_1\rangle\langle A_2A_1|). \tag{22}$$

In this case the reduced density operators are

$$\rho_{\rm sep,A} = \rho_{\rm sep,B} = \frac{1}{2}(|A_1\rangle\langle A_1| + |A_2\rangle\langle A_2|). \tag{23}$$

We also consider the entangled state $|s\rangle = \mathcal{N}(|A_1A_2\rangle + |A_2A_1\rangle)$ with density operator

$$\rho_{\rm ent} = 2\mathcal{N}^2\rho_{\rm sep} + \mathcal{N}^2(|A_1A_2\rangle\langle A_2A_1| + |A_2A_1\rangle\langle A_1A_2|) \tag{24}$$

where the normalization constant is given by

$$\mathcal{N} = \left[2 + 2\exp\left(-|A_1 - A_2|^2\right)\right]^{-1/2}. \tag{25}$$

In this case the reduced density operators are

$$\rho_{\rm ent,A} = \rho_{\rm ent,B} = \mathcal{N}^2(|A_1\rangle\langle A_1| + |A_2\rangle\langle A_2| + \chi|A_1\rangle\langle A_2| + \chi^*|A_2\rangle\langle A_1|) \tag{26}$$

where

$$\chi = \langle A_1|A_2\rangle = \exp\left(-\frac{|A_1|^2}{2} - \frac{|A_2|^2}{2} + A_1^*A_2\right). \tag{27}$$

3. Magnetic flux operator

We consider a monochromatic electromagnetic field of frequency ω, at sufficiently low temperatures $T \ll \omega$, so that the quantum noise is greater than the thermal noise. In this case the vector potential $\hat{A}_i$ and the electric field $\hat{E}_i$ are dual quantum variables. For a loop C, which is small in comparison to the wavelength of the electromagnetic field, the $\hat{A}_i, \hat{E}_i$ are integrated around C and yield the magnetic flux $\hat{\phi} = \oint_C \hat{A}_i dx_i$ and the electromotive force $\hat{V}_{\rm EMF} = \oint_C \hat{E}_i dx_i$, correspondingly, as dual quantum variables.

In terms of these variables the photon creation and annihilation operators are

$$\hat{a}^\dagger = \frac{1}{\sqrt{2}\xi}(\hat{\phi} - i\omega^{-1}\hat{V}_{\rm EMF}), \qquad \hat{a} = \frac{1}{\sqrt{2}\xi}\left(\hat{\phi} + i\omega^{-1}\hat{V}_{\rm EMF}\right), \tag{28}$$

where ξ is a constant proportional to the area enclosed by C. Consequently the magnetic flux operator is $\hat{\phi}(0) = 2^{-1/2}\xi(\hat{a}^\dagger + \hat{a})$ and its evolution in time is given by

$$\hat{\phi}(t) = \exp(it\mathcal{H})\hat{\phi}(0)\exp(-it\mathcal{H}). \tag{29}$$

The Hamiltonian $\mathcal{H}$ of the system is

$$\mathcal{H} = \omega(a^\dagger a + 1/2) + \mathcal{H}_{\rm int}. \tag{30}$$

In the external field approximation we ignore the interaction Hamiltonian $\mathcal{H}_{\rm int}$ and we obtain

$$\hat{\phi}(t) = \frac{\xi}{\sqrt{2}}\left[\exp(i\omega t)\hat{a}^\dagger + \exp(-i\omega t)\hat{a}\right]. \tag{31}$$

This is a good approximation when the flux due to back reaction is small in comparison to the external flux.

The expectation value of the flux and the quantum uncertainty $\Delta\hat{\phi}$ are given by

$$\langle\hat{\phi}(t)\rangle = \mathrm{Tr}[\rho\hat{\phi}(t)], \qquad \Delta\hat{\phi} = [\langle\hat{\phi}^2(t)\rangle - \langle\hat{\phi}(t)\rangle^2]^{1/2}. \tag{32}$$

For example, in the case of number states $\rho = |N\rangle\langle N|$ we get

$$\langle\hat{\phi}(t)\rangle_{\mathrm{num}} = 0, \qquad (\Delta\hat{\phi})_{\mathrm{num}} = \left(N + \frac{1}{2}\right)^{1/2}. \tag{33}$$

For coherent states $\rho = |A\rangle\langle A|$ we have

$$\langle\hat{\phi}(t)\rangle_{\mathrm{coh}} = 2^{1/2}|A|\cos(\omega t - \arg A), \qquad (\Delta\hat{\phi})_{\mathrm{coh}} = 2^{-1/2}. \tag{34}$$

In the case of squeezed states $\rho = |A; r\varphi\rangle\langle A; r\varphi|$ we obtain

$$\begin{aligned}
&\langle\hat{\phi}(t)\rangle_{\mathrm{sq}} = -2^{1/2}|A||Z|\cos(\omega t + \arg Z), \\
&(\Delta\hat{\phi})_{\mathrm{sq}} = 2^{-1/2}[\cosh(r) - \sinh(r)\cos(2\omega t + \varphi)]^{1/2}, \\
&Z = \sinh(r/2)\exp[i(\arg A + \varphi)] - \cosh(r/2)\exp(-i\arg A).
\end{aligned} \tag{35}$$

Finally for the thermal states of equation (8) we get

$$\langle\hat{\phi}(t)\rangle_{\mathrm{th}} = 0, \qquad (\Delta\hat{\phi})_{\mathrm{th}} = \frac{1}{\sqrt{2}}\left[\coth\left(\frac{1}{2}\beta\omega\right)\right]^{1/2}. \tag{36}$$

4. Aharonov-Bohm phase factor induced by a magnetostatic flux

We consider a two-path electron interference experiment, as shown in figure 2.

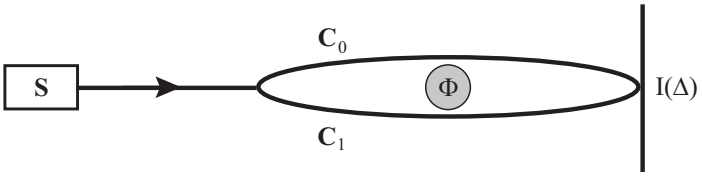

Figure 2. Aharonov-Bohm experiment. The electrons follow the lowest winding paths C_0, C_1 in a field-free region. The loop $C_0 - C_1$ is threaded by a magnetostatic flux Φ.

The wavefunctions corresponding to paths C_0 and C_1 are ψ_0 and ψ_1, respectively. In the presence of magnetic flux Φ threading the loop $C_0 - C_1$, we get the electron intensity

$$I(x) = |\psi_0|^2 + |\psi_1|^2 + 2|\psi_0\psi_1|\cos(x - e\Phi), \tag{37}$$

where x is the phase difference between the two paths:

$$x(\Delta) \equiv \arg(\psi_0) - \arg(\psi_1). \tag{38}$$

If we assume equal splitting (i.e., $|\psi_0|^2 = 1/2 = |\psi_1|^2$) then

$$I(x) = 1 + \cos(x - e\Phi). \tag{39}$$

The visibility of the intensity I, defined as

$$\nu = \frac{I_{\max} - I_{\min}}{I_{\max} + I_{\min}}, \tag{40}$$

is equal to one in this case.

5. Phase factor operator induced by nonclassical electromagnetic fields

In this section we consider a mesoscopic electron interference device ($\sim 0.1\mu$m) in a microwave waveguide at low temperatures ($10 - 100$mK). The electric field is parallel to the plane of the electron paths and the magnetic field is perpendicular to it (figure 3). The electron intensity is given by equation (37) where the flux Φ is now time-dependent.

We next consider the case where the microwaves are nonclassical. In this case Φ is a quantum mechanical operator and its expectation value with respect to the density matrix ρ of the microwaves gives the observed electron intensity:

$$I(x,t) = 1 + \mathrm{Tr}[\rho \cos(x - e\hat{\phi})] = 1 + \Re[\mathrm{e}^{ix}\tilde{W}(\lambda)] = 1 + |\tilde{W}(\lambda)| \cos\{x - \arg[\tilde{W}(\lambda)]\}. \quad (41)$$

Here $\tilde{W}$ is the Weyl function of the density matrix ρ defined in equation (10), and we define

$$\lambda = iq \exp(i\omega t), \qquad q = \frac{\xi e}{\sqrt{2}}. \quad (42)$$

If we compare and contrast equation (39) for classical microwaves, with equation (41) for nonclassical microwaves we see that the visibility is reduced in the second case from 1 to $|\tilde{W}(\lambda)|$. This is due to the quantum noise in the nonclassical microwaves as can be seen from the expansion

$$|\tilde{W}(\lambda)|^2 = 1 - \frac{q^2}{2}[(\Delta X)^2 + (\Delta P)^2] - \frac{q^2}{2}[(\Delta X)^2 - (\Delta P)^2]\cos(2\omega t) - \ldots \quad (43)$$

where $X = \xi^{-1}\hat{\phi}$, $P = (\omega\xi)^{-1}\hat{V}_{\mathrm{EMF}}$, and $\Delta X, \Delta P$ are the corresponding uncertainties. The $|\tilde{W}(\lambda)|$ is less than 1 due to the non-zero values of the quantum noise $\Delta X, \Delta P$.

Results are given below for the electron intensity $I(x,t)$ that corresponds to irradiation with several quantum states. We choose the point $x = 0$, for simplicity.

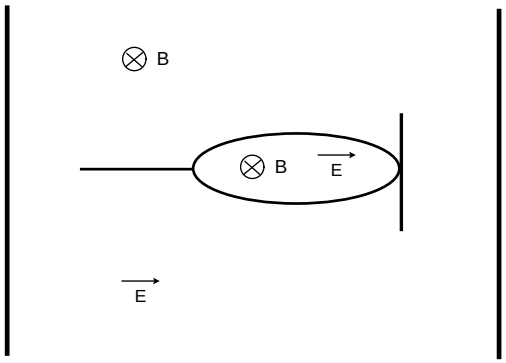

Figure 3. Modified Aharonov-Bohm experiment in the presence of an electromagnetic field. The field travels in the waveguide with the magnetic field perpendicular to the plane of the electron paths C_0, C_1 and the electric field parallel to it.

5.0.3. Number states For the number states of equation (2), using equation (13), we get

$$I_{\mathrm{num}}(t) = 1 + \exp\left(-\frac{q^2}{2}\right) L_N\left(q^2\right). \quad (44)$$

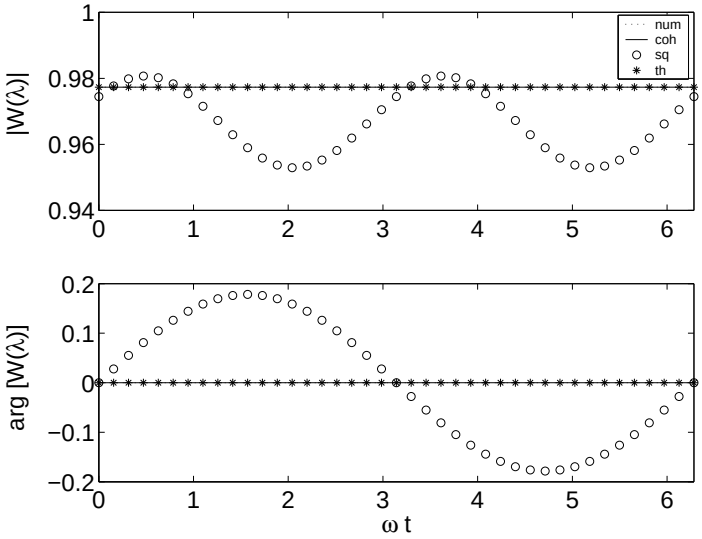

Figure 4. Vacuum-induced phase factor for the charges as a function of time, ωt, for $\omega = 10^{-4}$, corresponding to the case of number states (broken line), coherent states (solid line), squeezed states (line of circles), and thermal states (line of stars). The average number of photons $\langle N \rangle$ is zero; the squeezing parameter r is 0.5. In subplot (a) the $|\tilde{W}(\lambda)|$ is shown and in (b) the $\arg[\tilde{W}(\lambda)]$ is shown.

5.0.4. Coherent states For the coherent states of equation (3), using equation (14), we get

$$I_{\rm coh}(t) = 1 + \exp\left(-\frac{q^2}{2}\right)\cos\left[2q|A|\cos(\omega t - \arg A)\right]. \tag{45}$$

In this case the result is very similar to the classical result of equation (39) but the visibility is slightly reduced from 1 to $\exp\left(-\frac{q^2}{2}\right)$. The quantum noise of the coherent states slightly destroys the interference and reduces its visibility. Even in the absence of microwaves (vacuum state) we get a reduction in the visibility due to the vacuum noise.

In figure 4 we have plotted the expectation value of the phase factor operator, which is induced by the electromagnetic vacuum, the coherent states of equation (3), the squeezed states of equation (6) for $r = 0.5$, and the thermal states of equation (8).

5.0.5. Squeezed states For the squeezed states of equation (6), using equation (15), we get

$$I_{\rm sq}(t) = 1 + \exp(-Y_1)\cos(X_1), \tag{46}$$

$$Y_1 = \frac{q^2}{2}[\cosh(r) - \sinh(r)\cos(2\omega t + \varphi)],$$

$$X_1 = 2q|A|\left[\cosh\left(\frac{r}{2}\right)\cos(\omega t - \arg A) - \sinh\left(\frac{r}{2}\right)\cos(\omega t + \arg A + \varphi)\right].$$

We note that in the case of squeezed vacuum ($A = 0$) the intensity $I_{\rm sq}(t)$ contains all the frequencies $2K\omega$ where K is an integer (after a Fourier expansion). In contrast in the case of coherent states we get all the frequencies $K\omega$. The factor of 2 in the case of

squeezed vacuum is related with the fact that the squeezed vacuum is a superposition of even number states only. Therefore the electrons can only absorb an even number of photons (there are no odd number states in this quantum state). In this case the result is qualitatively different from the classical result.

5.0.6. Thermal states For the thermal states of equation (8), using equation (16), we have

$$I_{\rm th}(t) = 1 + \exp\left[-\frac{q^2}{2}\coth\left(\frac{\beta\omega}{2}\right)\right]. \tag{47}$$

6. Quantum statistics of the interfering electrons

There are various quantities that can be used to describe the quantum statistics of the interfering electrons. In the previous section we studied the electron intensity and here we consider higher order correlations [10]. We compare and contrast the results for the two cases of classical and nonclassical microwaves.

6.1. Autocorrelation function of the electron intensity in the case of classical microwaves

In general for a function $I(t)$ the autocorrelation function is defined as

$$\Gamma(\tau) = \lim_{T\to\infty}\frac{1}{2T}\int_{-T}^{T} I^*(t)I(t+\tau)dt. \tag{48}$$

The following properties are well known (e.g., see reference [35]):

$$\Gamma(-\tau) = \Gamma^*(\tau), \qquad \Gamma(0) \geq 0, \qquad |\Gamma(\tau)| \leq \Gamma(0). \tag{49}$$

The normalized autocorrelation function is defined as

$$\gamma(\tau) \equiv \frac{\Gamma(\tau)}{\Gamma(0)}, \qquad 0 \leq |\gamma(\tau)| \leq 1. \tag{50}$$

An expansion of $\Gamma(\tau)$ into a Fourier series yields the spectral density coefficients

$$\begin{aligned} S_K &= \frac{\Omega}{2\pi}\int_0^{2\pi/\Omega}\Gamma(\tau)\exp(-iK\Omega\tau)d\tau \\ \Gamma(\tau) &= \sum_{K=-\infty}^{\infty} S_K\exp(iK\Omega\tau). \end{aligned} \tag{51}$$

The property $\Gamma(-\tau) = \Gamma^*(\tau)$ of equation (49) guarantees that the coefficients S_K are real numbers. If the autocorrelation function is purely real then the spectral density coefficients obey the relation $S_K = S_{-K}$. But if $\Gamma(\tau)$ is complex then, in general, $S_K \neq S_{-K}$ and we refer to this as an asymmetry in the spectral density.

As an example we consider classical microwaves of frequency ω with magnetic flux of the form

$$\phi(t) = \phi_1\sin(\omega t). \tag{52}$$

In this case the electron intensity at the point $x = 0$ on the screen is

$$I_{\rm cl}(t) = 1 + \cos[e\phi_1 \sin(\omega t)]. \tag{53}$$

Therefore the autocorrelation function is

$$\Gamma_{\rm cl}(\tau) = [1 + J_0(e\phi_1)]^2 + 2\sum_{K=1}^{\infty} [J_{2K}(e\phi_1)]^2 \cos(2K\omega\tau), \tag{54}$$

where the $J_n(z)$ are Bessel functions [34], and the spectral density coefficients are

$$S_0 = [1 + J_0(e\phi_1)]^2, \qquad S_K = [J_{2K}(e\phi_1)]^2. \tag{55}$$

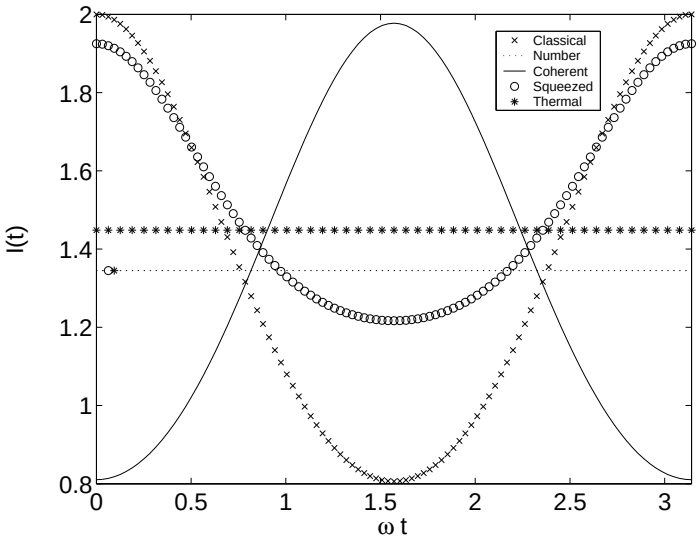

Figure 5. $I(0,t)$ for the electrons as a function of time, ωt, for $\omega = 10^{-4}$, corresponding to irradiation with number states (broken line), coherent states (solid line), squeezed states (line of circles), and thermal states (line of stars). We have chosen $\langle N\rangle = 17$, in all four cases, and $r = 4.2$ for the squeezed states. For comparison, we also show the electron intensity of equation (53) corresponding to classical microwaves (line of crosses), for $\phi_1 = (2\langle N\rangle)^{1/2}$.

6.2. Autocorrelation function of the electron intensity in the case of nonclassical microwaves

In this case the electron intensity $\hat{I}(t) = 1 + \cos[e\hat{\phi}(t)]$ is an operator. Consequently the autocorrelation function $\Gamma(\tau)$ of equation (48) is in this case defined as

$$\Gamma(\tau) = \lim_{T\to\infty} \frac{1}{2T} \int_{-T}^{T} {\rm Tr}[\rho \hat{I}^{\dagger}(t)\hat{I}(t+\tau)]dt. \tag{56}$$

The values of $\Gamma(\tau)$ for the electric charges have been derived for irradiation with various nonclassical microwave states in [10]. In the following we present numerical results, which illustrate the electron correlation properties, and allow for a comparison between the effects of classical and nonclassical microwaves.

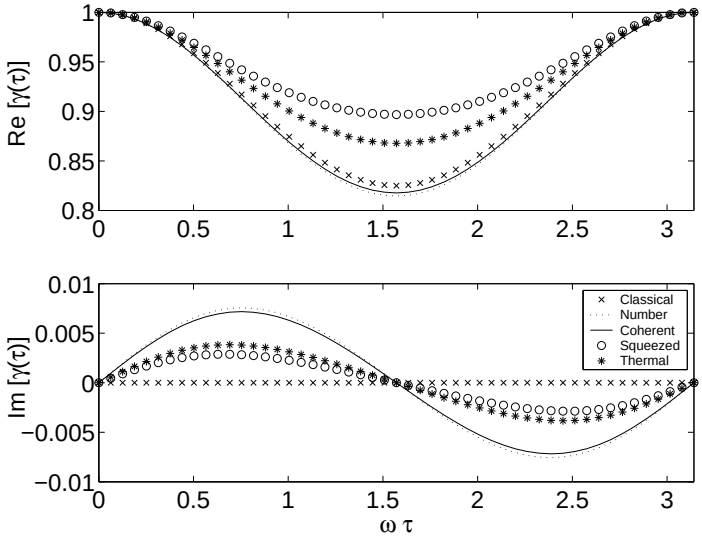

Figure 6. Real and imaginary parts of $\gamma(\tau)$ of equation (50) for the electrons as a function of time, $\omega\tau$, for $\omega = 10^{-4}$, corresponding to irradiation with number states (broken line), coherent states (solid line), squeezed states (line of circles), and thermal states (line of stars). The parameters are $\langle N\rangle = 17$, $r = 4.2$, and for the case of classical microwaves (line of crosses) we have $\phi_1 = (2\langle N\rangle)^{1/2}$.

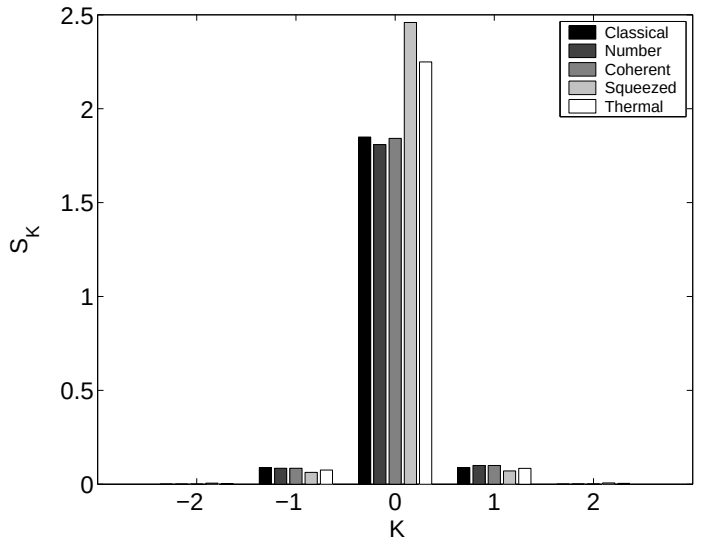

Figure 7. Spectral density coefficients S_K of equation (51) for the electrons as a function of K, corresponding to irradiation with classical microwaves (first column from the left), and nonclassical microwaves in number states (second column), coherent states (third column), squeezed states (fourth column), and thermal states (fifth column). The parameters are $\langle N\rangle = 17$, $r = 4.2$, and $\phi_1 = (2\langle N\rangle)^{1/2}$.

6.3. Numerical results

In order to make the comparison meaningful, in the numerical calculations (figures 5-7) the number of photons in the number states is equal to the average number of photons

in the coherent, squeezed, and thermal states; we have chosen

$$N = \langle N\rangle_{\rm coh} = \langle N\rangle_{\rm sq} = \langle N\rangle_{\rm th} = 17. \tag{57}$$

For comparison with the case of classical microwaves we have chosen the amplitude of the classical magnetic flux to be $\phi_1 = (2\langle N\rangle)^{1/2}$. The frequency of the microwaves is $\omega = 10^{-4}$ in units where $k_B = \hbar = c = 1$. The squeezing parameter is $r = 4.2$ and the other parameters are $\xi = 1$, $\arg A = 0$, $\varphi = 0$.

In figure 5 we show the electron intensity $I(t)$ for $x = 0$ as a function of ωt for irradiation with number states (broken line), coherent states (solid line), squeezed states (line of circles), and thermal states (line of stars). For comparison, we also show the electron intensity of equation (53) corresponding to classical microwaves (line of crosses).

In figure 6 we show the real and imaginary parts of $\gamma(\tau)$ of equation (50) for the electrons as a function of $\omega\tau$ corresponding to irradiation with number states (broken line), coherent states (solid line), squeezed states (line of circles), and thermal states (line of stars); we have also included the results in the case of classical microwaves (line of crosses) for comparison. It is seen that different states of the electromagnetic field lead to different electron correlation properties. The imaginary part of the normalized autocorrelation function vanishes only for irradiation with classical microwaves, but it is nonzero for the four cases of nonclassical microwaves.

In figure 7 we plot the spectral density coefficients S_K of equation (51) for the electrons as a function of K, corresponding to irradiation with classical microwaves (first column from the left), and nonclassical microwaves in number states (second column), coherent states (third column), squeezed states (fourth column), and thermal states (fifth column).

7. Entangled currents in distant electron interference experiments induced by entangled photons

In this section we consider two electron interference devices that are far from each other [19]. A photon source irradiates the two experiments with correlated two-mode nonclassical microwaves. Each microwave field mode is coupled to one of the two experiments. The experiment is depicted in figure 8. It will be shown that the photon correlations are transferred to the electron interference experiments, which become correlated. The nature of their correlation depends on whether the external photons are separable (classically correlated) or entangled (quantum mechanically correlated).

Let ρ be the density operator describing the two-mode nonclassical electromagnetic field. The first mode of frequency ω_1 interacts with electrons in experiment **A** and its density matrix is given by $\rho_{\rm A} = {\rm Tr}_{\rm B}(\rho)$. Similarly the second mode of frequency ω_2 interacts with electrons in experiment **B** and its density matrix is $\rho_{\rm B} = {\rm Tr}_{\rm A}(\rho)$. The density matrix ρ can be factorizable (i.e., the field modes are independent of each other), separable (the field modes are classically correlated), or entangled (the field modes are quantum mechanically correlated). The difference between these cases has been discussed in section 2.

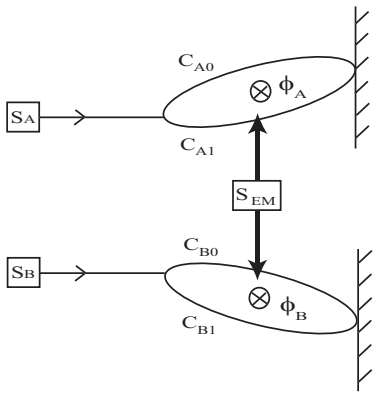

Figure 8. Two electron interference experiments which are far from each other are irradiated with nonclassical electromagnetic fields. The two electromagnetic fields in the two experiments are produced by the source $S_{\rm EM}$ and are correlated.

7.1. Correlations of the electron intensity distributions

The nonclassical magnetic flux $\hat{\phi}_{\rm A}$ that influences the electron interference in **A** gives rise to the phase factor operator $\exp(ie\hat{\phi}_{\rm A})$. This phase factor induces the electron intensity distribution $I_{\rm A}(x_{\rm A})$, which is given by

$$I_{\rm A}(x_{\rm A}) = {\rm Tr}\{\rho_{\rm A}[1+\cos(x_{\rm A}-e\hat{\phi}_{\rm A})]\} = 1+|\tilde{W}(\lambda_{\rm A})|\cos\{x_{\rm A}-\arg[\tilde{W}(\lambda_{\rm A})]\} \tag{58}$$

where $\lambda_{\rm A} = iq\exp(i\omega_1 t)$. Similarly in experiment **B**, which is influenced by a nonclassical magnetic flux $\hat{\phi}_{\rm B}$, one obtains the intensity

$$I_{\rm B}(x_{\rm B}) = {\rm Tr}\{\rho_{\rm B}[1+\cos(x_{\rm B}-e\hat{\phi}_{\rm B})]\} = 1+|\tilde{W}(\lambda_{\rm B})|\cos\{x_{\rm B}-\arg[\tilde{W}(\lambda_{\rm B})]\} \tag{59}$$

where $\lambda_{\rm B} = iq\exp(i\omega_2 t)$.

The electron intensity on the interference screen of experiment **A** (or **B**) is calculated by tracing the intensity operator with respect to the density matrix that describes the corresponding electromagnetic field mode ($\rho_{\rm A}$ or $\rho_{\rm B}$). The results, $I_{\rm A}(x_{\rm A})$ and $I_{\rm B}(x_{\rm B})$, are proportional to the probability of detecting an electron at a point $x_{\rm A}$ in **A** or a point $x_{\rm B}$ in **B**. It is also possible to define the joint electron intensity $I(x_{\rm A},x_{\rm B})$, which is related to the probability of a simultaneous detection of electrons at $x_{\rm A}$ and $x_{\rm B}$. This joint intensity is controlled by the full density matrix ρ for the two-mode electromagnetic field, that is,

$$I(x_{\rm A},x_{\rm B}) = {\rm Tr}\{\rho[1+\cos(x_{\rm A}-e\hat{\phi}_{\rm A})][1+\cos(x_{\rm B}-e\hat{\phi}_{\rm B})]\}. \tag{60}$$

If the two-mode electromagnetic field is factorizable ($\rho = \rho_{\rm A}\otimes\rho_{\rm B}$) then the joint electron intensity $I(x_{\rm A},x_{\rm B})$ is simply equal to the product $I_{\rm A}(x_{\rm A})I_{\rm B}(x_{\rm B})$ of the independent intensities. However, if the two field modes are classically or quantum mechanically correlated then this is not true, in general. In order to quantify this we can define the ratio

$$R = \frac{I(x_{\rm A},x_{\rm B})}{I_{\rm A}(x_{\rm A})I_{\rm B}(x_{\rm B})} \tag{61}$$

which is equal to one only for independent electron intensities. In other words, whenever R takes values not equal to one, the electron intensity in experiment **A** is correlated to the electron intensity in experiment **B**. In what follows we consider particular examples that illustrate the effect.

7.2. Examples and numerical results

As an example we consider two-mode separable and entangled microwaves in number states[19]. We compare and contrast the effects of the separable state

$$\rho_{\rm sep} = \frac{1}{2}(|00\rangle\langle 00| + |11\rangle\langle 11|) \tag{62}$$

and the entangled state $2^{-1/2}(|00\rangle + |11\rangle)$ with density matrix

$$\rho_{\rm ent} = \rho_{\rm sep} + \frac{1}{2}(|00\rangle\langle 11| + |11\rangle\langle 00|). \tag{63}$$

It is noted that the $\rho_{\rm sep}$ and the $\rho_{\rm ent}$ differ only in the above nondiagonal elements. The reduced density operators that describe the electromagnetic field in **A** and **B** are, in both cases,

$$\rho_{\rm sep,A} = \rho_{\rm ent,A} = \rho_{\rm sep,B} = \rho_{\rm ent,B} = \frac{1}{2}(|0\rangle\langle 0| + |1\rangle\langle 1|). \tag{64}$$

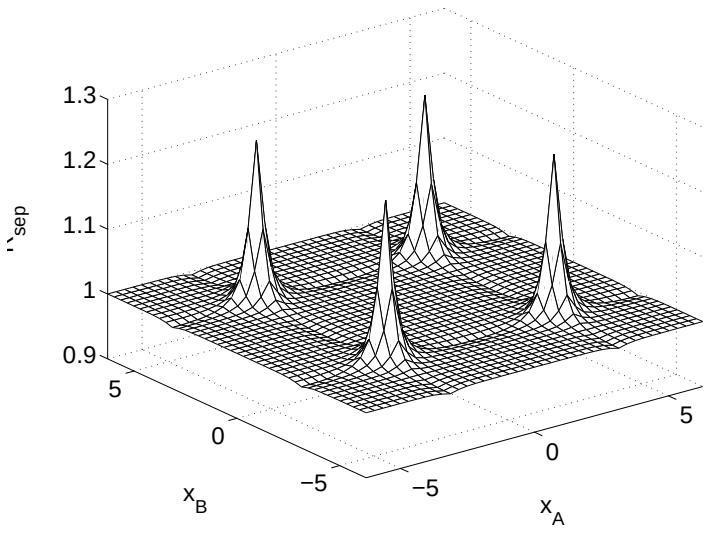

Figure 9. $R_{\rm sep}$ of equation (65) as a function of $x_{\rm A}, x_{\rm B} \in [-2\pi, 2\pi]$. Here $\min(R_{\rm sep}) = 1.0001$ and $\max(R_{\rm sep}) = 1.2471$. The frequencies are $\omega_1 = 1.2 \times 10^{-4}$ and $\omega_2 = 10^{-4}$.

The ratio of equation (61) corresponding to the separable state $\rho_{\rm sep}$ is given by

$$R_{\rm sep}(x_{\rm A}, x_{\rm B}) = \frac{1 + \alpha(\cos x_{\rm A} + \cos x_{\rm B}) + \gamma \cos x_{\rm A} \cos x_{\rm B}}{(1 + \alpha \cos x_{\rm A})(1 + \alpha \cos x_{\rm B})} \tag{65}$$

where

$$\alpha = \frac{2-q^2}{2}\exp\left(-\frac{q^2}{2}\right), \qquad \gamma = \frac{1}{2}\exp(-q^2)[1+(1-q^2)^2]. \tag{66}$$

It can easily be shown that

$$\frac{1+2\alpha+\gamma}{(1+\alpha)^2} \leq R_{\rm sep}(x_{\rm A}, x_{\rm B}) \leq \frac{1-2\alpha+\gamma}{(1-\alpha)^2} \tag{67}$$

which in our example leads to $\min(R_{\rm sep}) = 1.0001$ and $\max(R_{\rm sep}) = 1.2471$. In figure 9 we plot the $R_{\rm sep}(x_{\rm A}, x_{\rm B})$ against screen positions $x_{\rm A}$ and $x_{\rm B}$ for microwave frequencies $\omega_1 = 1.2\times10^{-4}$ and $\omega_2 = 10^{-4}$.

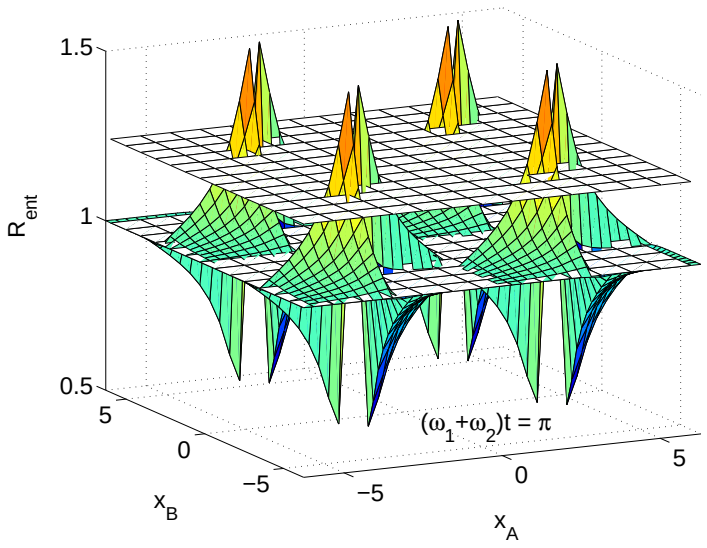

Figure 10. $R_{\rm ent}$ of equation (68) as a function of $x_{\rm A}, x_{\rm B} \in [-2\pi, 2\pi]$ for $(\omega_1+\omega_2)t = \pi$. The top and bottom plateaus show the $\max(R_{\rm sep}) = 1.2471$ and $\min(R_{\rm sep}) = 1.0001$, respectively. The frequencies are $\omega_1 = 1.2\times10^{-4}$ and $\omega_2 = 10^{-4}$.

In the case of the entangled state $\rho_{\rm ent}$ of equation (63) the ratio is

$$R_{\rm ent}(x_{\rm A}, x_{\rm B}, t) = R_{\rm sep}(x_{\rm A}, x_{\rm B}) - q^2\exp(-q^2)\frac{\sin x_{\rm A}\sin x_{\rm B}\cos[(\omega_1+\omega_2)t]}{(1+\alpha\cos x_{\rm A})(1+\alpha\cos x_{\rm B})}. \tag{68}$$

The $R_{\rm ent}$ oscillates in time around the $R_{\rm sep}$, with frequency $\omega_1+\omega_2$, and exceeds periodically the bounds of the inequality for $R_{\rm sep}$ in (67). In figure 10 we plot the $R_{\rm ent}(x_{\rm A}, x_{\rm B})$ against screen positions $x_{\rm A}$ and $x_{\rm B}$ for $(\omega_1+\omega_2)t = \pi$ and the same microwave frequencies as in the previous figure. The two horizontal surfaces represent the $\min(R_{\rm sep})$ (bottom plateaux) and the $\max(R_{\rm sep})$ (top plateaux). In figure 11 we compare the $R_{\rm sep}$ (line of circles) and the $R_{\rm ent}$ (solid line) against time $(\omega_1+\omega_2)t$ for fixed screen positions $x_{\rm A} = 0.9\pi$ and $x_{\rm B} = 1.025\pi$.

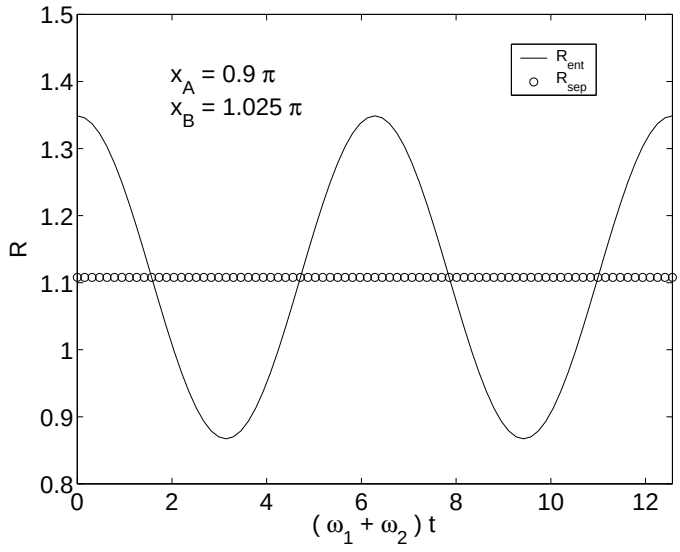

Figure 11. Comparison of $R_{\rm ent}$ (solid line) and $R_{\rm sep}$ (line of circles) of equations (68) and (65), respectively, for $x_{\rm A} = 0.9\pi$ and $x_{\rm B} = 1.025\pi$ as a function of dimensionless time. The frequencies are $\omega_1 = 1.2 \times 10^{-4}$ and $\omega_2 = 10^{-4}$.

8. Interaction of mesoscopic SQUID rings with nonclassical electromagnetic fields

In this section we investigate application of the above ideas in the context of mesoscopic superconducting quantum interference device (SQUID) rings. In the first instance we introduce mesoscopic SQUID rings and describe how they interact with nonclassical electromagnetic fields [25, 26]. In this case the Josephson currents are quantum mechanical operators, whose expectation values with respect to the density operator of the external photons, yield the observed currents. Subsequently, we apply the general concept described in the previous section to the case of two distant SQUID rings, each of which is coupled to a single mode of a two-mode nonclassical electromagnetic field [29]. It is shown that the photon correlations are transferred to the Josephson currents in the distant superconducting devices.

8.1. Mesoscopic SQUID ring

Consider a superconducting ring of mesoscopic area $\xi \leq 10^{-8}{\rm cm}^2$, which is interrupted by a Josephson junction (weak link), as shown in the figure below. In this case the capacitance C across the Josephson junction is very small and at low temperatures $T < 0.1K$ the behaviour of the SQUID is nonclassical [22] in the sense that the Coulomb charging energy for a Cooper pair of charge $2e$,

$$E_C = \frac{(2e)^2}{C}, \tag{69}$$

becomes a significant parameter.

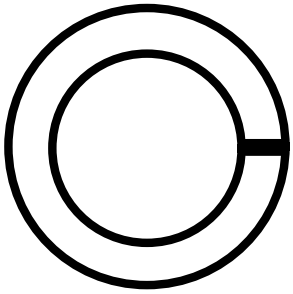

Figure 12. Mesoscopic SQUID ring: superconducting ring of mesoscopic dimensions is interrupted by a Josephson junction.

Under these conditions the charge $\hat{Q} = -i(2e)\partial_\delta$ through the junction and the phase difference across the junction $\hat{\delta}$ are conjugate operators, which obey the commutation relation $[\hat{\delta}, \hat{Q}] = i2e$. In this case the Josephson current also becomes an operator which is a sinusoidal function of the phase difference across the junction,

$$\hat{I} = I_{\rm c} \sin \hat{\delta}, \tag{70}$$

where $I_{\rm c}$ is the critical current.

8.2. Interaction with classical microwaves

We consider a mesoscopic SQUID ring interacting with a monochromatic electromagnetic field. The magnetic flux $\phi(t)$ is threading the SQUID ring and the phase difference across the junction is $\delta = 2e\phi(t)$.

In the classical case the Josephson current I and the phase difference δ, are classical numbers. Therefore for a magnetic flux with a linear and a sinusoidal component,

$$\phi(t) = \phi_0 + V_1 t + u \sin(\omega_1 t), \tag{71}$$

we get the current

$$I = I_1 \sin[2e\phi(t)] = I_1 \sin[2e\phi_0 + 2eV_1 t + 2eu \sin(\omega_1 t)]. \tag{72}$$

Using the well-known identity

$$\exp(iu \sin z) = \sum_{n=-\infty}^{\infty} J_n(u) \exp(inz), \tag{73}$$

we can easily show that the current can be expanded as

$$I = I_1 \sum_{n=-\infty}^{\infty} J_n(2eu) \sin[(2eV_1 + n\omega_1)t + 2e\phi_0]. \tag{74}$$

Calculating the time-averaged value $I_{\rm dc}$ of the current I we see that when

$$2eV_0 = N\omega \tag{75}$$

where N is an integer, we get

$$I_{\rm dc} = I_1 J_{-N}(2eu) \sin(2e\phi_0), \tag{76}$$

otherwise the $I_{\rm dc}$ vanishes. These integral values of the voltage are usually referred to as Shapiro steps.

8.3. Interaction with nonclassical microwaves

We now study the effect of nonclassical microwaves on the Josephson current of a mesoscopic SQUID ring operating at low temperatures.We use the external field approximation, and ignore the back-reaction. This is a good approximation when the external electromagnetic fields are much stronger than the fields induced by the currents circulating the mesoscopic devices.

We consider the irradiation of a mesoscopic SQUID ring with monochromatic nonclassical microwaves of frequency ω_1. In addition to that the ring is threaded by the classical flux $\phi_0 + V_1 t$ and the total flux is $\hat{\Phi}(t) = \phi_0 + V_1 t + \hat{\phi}(t)$. Therefore the quantum current is in this case given by

$$\begin{aligned}\hat{I}_{\rm A} &= I_1 \sin\left\{2e\phi_0 + 2eV_1 t + q'\left[\exp(i\omega_1 t)\hat{a}^\dagger + \exp(-i\omega_1 t)\hat{a}\right]\right\} \\ &= I_1 \Im\left\{\exp[i(\omega_A t + 2e\phi_0)] D[iq'\exp(i\omega_1 t)]\right\} \end{aligned} \tag{77}$$

where

$$\omega_A = 2eV_1, \qquad q' = \sqrt{2}e\xi. \tag{78}$$

It is noted that the scaled electric charge q' has twice the value of q of equation (42), because in this case we have pairs of electrons. The experimentally measured current is calculated by tracing with respect to the density operator $\rho_{\rm A}$ for the external electromagnetic fields, that is,

$$\langle I_{\rm A}\rangle \equiv {\rm Tr}(\rho_{\rm A}\hat{I}_{\rm A}) = I_1 \Im[\exp(i\omega_{\rm A} t)\tilde{W}(\sigma_{\rm A})], \qquad \sigma_{\rm A} = iq'\exp(i\omega_1 t). \tag{79}$$

As an example we consider microwaves in coherent states. For comparison with the classical case of equation (76) we take coherent states with $A = 2^{-1/2}u$ and $\arg A = 0$. In this case we get Shapiro steps, as in the classical case, but the dc current is now reduced by a small factor:

$$I_{\rm dc}^{\rm (coh)} = \exp\left(-\frac{q'^2}{2}\right) I_{\rm dc}. \tag{80}$$

We also consider the case where the microwaves are in a squeezed vacuum. The squeezed vacuum is a superposition of even number states only. In this case [25] we get even Shapiro steps only. A physical interpretation of this result is that the electrons can only absorb an even number of photons (there are no odd number states in this quantum state). Similar results can be proved for even Schroedinger cats ($\mathcal{N}(|A\rangle + |-A\rangle)$), which are superpositions of even number states also. We stress that in this case the result is qualitatively different from the classical result, in the sense that the odd Shapiro steps are absent.

8.4. Entanglement of distant mesoscopic SQUID rings

We consider two spatially separated mesoscopic SQUID rings, which we refer to as A and B. They are irradiated with microwaves that are described by a density operator ρ. The microwaves are produced by the same source and are correlated. Photons of frequency

ω_1 interact with device A;and photons of frequency ω_2 interact with device B. The SQUID rings A and B are also threaded by a classical time-dependent magnetic fluxes that increase linearly with time ($V_{\rm A}t$ and $V_{\rm B}t$, respectively). The proposed experiment is illustrated in figure 13.

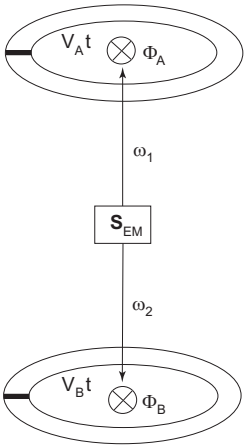

Figure 13. Two distant mesoscopic SQUID rings A and B are irradiated with nonclassical microwaves of frequencies ω_1 and ω_2, respectively. The microwaves are produced by the source $\rm S_{EM}$ and are correlated. Classical magnetic fluxes $V_{\rm A}t$ and $V_{\rm B}t$ are also threading the two rings A and B, respectively.

The observed Josephson current in SQUID ring A or B is given by the expectation value of the corresponding current operator,

$$\langle \hat{I}_{\rm A}\rangle = I_1 {\rm Tr}(\rho_{\rm A} \sin\hat{\delta}_{\rm A}), \qquad \hat{\delta}_{\rm A} = 2eV_{\rm A}t + 2e\hat{\phi}_{\rm A}(t), \tag{81}$$

$$\langle \hat{I}_{\rm B}\rangle = I_2 {\rm Tr}(\rho_{\rm B} \sin\hat{\delta}_{\rm B}), \qquad \hat{\delta}_{\rm B} = 2eV_{\rm B}t + 2e\hat{\phi}_{\rm B}(t), \tag{82}$$

where

$$\hat{\phi}_{\rm A}(t) = \frac{\xi}{\sqrt{2}}\left[\exp(i\omega_1 t)\hat{a_1}^\dagger + \exp(-i\omega_1 t)\hat{a_1}\right], \tag{83}$$

$$\hat{\phi}_{\rm B}(t) = \frac{\xi}{\sqrt{2}}\left[\exp(i\omega_2 t)\hat{a_2}^\dagger + \exp(-i\omega_2 t)\hat{a_2}\right], \tag{84}$$

in accordance with the formalism developed in section 3 and assuming that both rings have the same area ξ. The $\langle \hat{I}_{\rm A}\rangle$ has been written in terms of the Weyl function $\tilde{W}(\sigma_{\rm A})$ in equation (79); and similarly for B.

The expectation value of the product of the two current operators is given by:

$$\langle \hat{I}_{\rm A}\hat{I}_{\rm B}\rangle = I_1 I_2 {\rm Tr}(\rho \sin\hat{\delta}_{\rm A} \sin\hat{\delta}_{\rm B}). \tag{85}$$

The correlations between the observed electron currents can be quantified by defining the ratio

$$R^{(\rm c)} = \frac{\langle \hat{I}_{\rm A}\hat{I}_{\rm B}\rangle}{\langle \hat{I}_{\rm A}\rangle\langle \hat{I}_{\rm B}\rangle}, \tag{86}$$

where the superscript (c) indicates that this quantity corresponds to currents. For factorizable density matrices $\rho_{\rm fact} = \rho_A \otimes \rho_B$ we easily obtain the ratio $R^{(\rm c)}_{\rm fact} = 1$, identically. For separable density matrices $\rho_{\rm sep}$ of equation (18) we get

$$R^{(\rm c)}_{\rm sep} = \frac{\sum_i p_i \langle \hat{I}_{{\rm A}i}\rangle \langle \hat{I}_{{\rm B}i}\rangle}{(\sum_k p_k \langle \hat{I}_{{\rm A}k}\rangle)(\sum_l p_l \langle \hat{I}_{{\rm B}l}\rangle)}. \tag{87}$$

We also calculate the higher moments of the currents

$$\langle \hat{I}^2_{\rm A}\rangle = I_1^2 {\rm Tr}[\rho_{\rm A}(\sin\hat{\sigma}_{\rm A})^2], \tag{88}$$

$$\langle \hat{I}^2_{\rm B}\rangle = I_2^2 {\rm Tr}[\rho_{\rm B}(\sin\hat{\sigma}_{\rm B})^2], \tag{89}$$

$$\langle \hat{I}^2_{\rm A}\hat{I}^2_{\rm B}\rangle = I_1^2 I_2^2 {\rm Tr}[\rho(\sin\hat{\sigma}_{\rm A})^2(\sin\hat{\sigma}_{\rm B})^2]. \tag{90}$$

The expectation value $\langle \hat{I}^M_{\rm A}\hat{I}^N_{\rm B}\rangle$ quantifies the quantum statistics of the electron pairs tunneling the junctions in the two SQUID rings. Consequently the ratio

$$R^{(\rm c2)} = \frac{\langle \hat{I}^2_{\rm A}\hat{I}^2_{\rm B}\rangle}{\langle \hat{I}^2_{\rm A}\rangle\langle \hat{I}^2_{\rm B}\rangle} \tag{91}$$

is a measure of the photon-induced correlations of the quantum statistics of the tunneling electrons. For factorizable density matrices we easily see that $R^{(\rm c2)}_{\rm fact} = 1$. For separable density matrices we get

$$R^{(\rm c2)}_{\rm sep} = \frac{\sum_i p_i \langle \hat{I}^2_{{\rm A}i}\rangle \langle \hat{I}^2_{{\rm B}i}\rangle}{(\sum_k p_k \langle \hat{I}^2_{{\rm A}k}\rangle)(\sum_l p_l \langle \hat{I}^2_{{\rm B}l}\rangle)}. \tag{92}$$

8.5. Examples and numerical results

We present examples in which we compare and contrast the influence of a classically correlated two-mode microwave state with a quantum mechanically correlated one, on the Josephson currents. The two-mode microwaves are in both number and coherent states.

8.5.1. Number states Firstly we consider the separable density operator $\rho_{\rm sep}$ of equation (19) and the entangled density operator $\rho_{\rm ent}$ of equation (20) for number states.

For the $\rho_{\rm sep}$ of equation (19) we calculate the currents in A and B:

$$\langle \hat{I}_{\rm A}\rangle = I_1 C_0 \sin(\omega_{\rm A} t), \tag{93}$$

$$\langle \hat{I}_{\rm B}\rangle = I_2 C_0 \sin(\omega_{\rm B} t), \tag{94}$$

$$C_0 = \frac{1}{2}\exp\left(-\frac{q'^2}{2}\right)[L_{N_1}(q'^2) + L_{N_2}(q'^2)], \tag{95}$$

where the $L^{\alpha}_n(x)$ are Laguerre polynomials [34]. It is noted that in this case the currents $\langle \hat{I}_{\rm A}\rangle, \langle \hat{I}_{\rm B}\rangle$ are independent of the microwave frequencies ω_1, ω_2. The second moments of the currents in A and B, defined by equations (88) and (89), respectively, have also been calculated:

$$\langle \hat{I}^2_{\rm A}\rangle = \frac{I_1^2}{2}[1 - C_1\cos(2\omega_{\rm A} t)], \tag{96}$$

$$\langle \hat{I}_{\rm B}^2 \rangle = \frac{I_2^2}{2}[1 - C_1 \cos(2\omega_{\rm B} t)], \tag{97}$$

$$C_1 \quad = \frac{1}{2} \exp(-2q^{'2})[L_{N_1}(4q^{'2}) + L_{N_2}(4q^{'2})]. \tag{98}$$

The expectation value of the product of the two currents is

$$\langle \hat{I}_{\rm A} \hat{I}_{\rm B} \rangle_{\rm sep} = I_1 I_2 C_2 \sin(\omega_{\rm A} t) \sin(\omega_{\rm B} t), \tag{99}$$

$$C_2 \qquad = \exp(-q^{'2}) L_{N_1}(q^{'2}) L_{N_2}(q^{'2}). \tag{100}$$

Consequently the ratio $R^{(c)}$ of equation (86) is

$$R_{\rm sep}^{(c)} = \frac{C_2}{C_0^2} = \frac{4 L_{N_1}(q^{'2}) L_{N_2}(q^{'2})}{[L_{N_1}(q^{'2}) + L_{N_2}(q^{'2})]^2}. \tag{101}$$

In this example the $R_{\rm sep}^{(c)}$ is time-independent; it depends only on the number of photons N_1, N_2 in the two-mode microwave field.

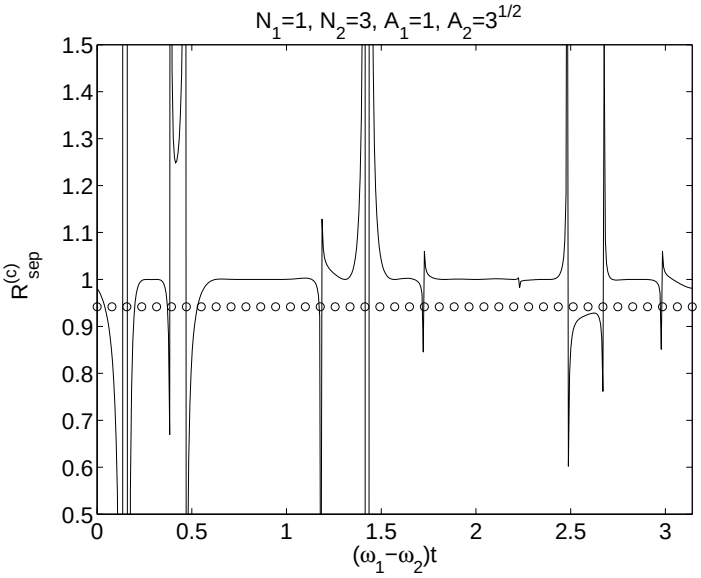

Figure 14. Comparison of $R_{\rm sep}^{(c)}$ for the separable number state of equation (19) (line of circles) and $R_{\rm sep}^{(c)}$ for the separable coherent state of equation (22) (solid line) for $N_1 = 1, N_2 = 3$ and $A_1 = 1, A_2 = 3^{1/2}$ as a function of $(\omega_1 - \omega_2)t$, where $\omega_1 = 1.2 \times 10^{-4}$ and $\omega_2 = 10^{-4}$.

For the $\rho_{\rm ent}$ of equation (20) the $\langle \hat{I}_{\rm A} \rangle, \langle \hat{I}_{\rm B} \rangle$ are the same with those presented in equations (93), (94); and the $\langle \hat{I}_{\rm A}^2 \rangle, \langle \hat{I}_{\rm B}^2 \rangle$ are the same as in equations (96), (97). However the $\langle \hat{I}_{\rm A} \hat{I}_{\rm B} \rangle$ is in this case

$$\langle \hat{I}_{\rm A} \hat{I}_{\rm B} \rangle_{\rm ent} = \langle \hat{I}_{\rm A} \hat{I}_{\rm B} \rangle_{\rm sep} + I_{\rm cross}, \tag{102}$$

where

$$I_{\rm cross} = \; - I_1 I_2 C_3 [\cos(\omega_{\rm A} t + \omega_{\rm B} t) - (-1)^{N_1 - N_2} \cos(\omega_{\rm A} t - \omega_{\rm B} t)] \cos(\Omega t), \tag{103}$$

$$C_3 \quad = \frac{1}{2} \exp(-q^{'2}) L_{N_1}^{N_2 - N_1}(q^{'2}) L_{N_2}^{N_1 - N_2}(q^{'2}). \tag{104}$$

The $I_{\rm cross}$ causes the $\langle \hat{I}_{\rm A}\hat{I}_{\rm B}\rangle_{\rm ent}$ to oscillate in time around the $\langle \hat{I}_{\rm A}\hat{I}_{\rm B}\rangle_{\rm sep}$ with frequency

$$\Omega = (N_1 - N_2)(\omega_1 - \omega_2). \tag{105}$$

We note that the term $I_{\rm cross}$ is induced by the nondiagonal elements of $\rho_{\rm ent}$ of equation (20), and depends on the photon frequencies ω_1, ω_2. This term quantifies the difference between the effect of separable and entangled microwaves on the Josephson currents.

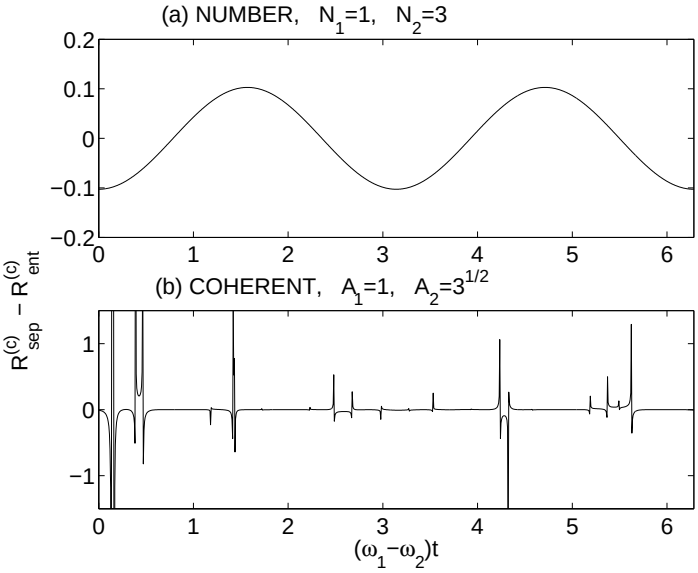

Figure 15. The difference $R^{(c)}_{\rm sep} - R^{(c)}_{\rm ent}$ corresponding to (a) the separable and entangled number states of equations (19), (20); and (b) the separable and entangled coherent states of equations (22), (24), for $N_1 = 1, N_2 = 3$ and $A_1 = 1, A_2 = 3^{1/2}$ as a function of $(\omega_1 - \omega_2)t$, where $\omega_1 = 1.2 \times 10^{-4}$ and $\omega_2 = 10^{-4}$.

In the entangled case the ratio $R^{(c)}$ of equation (86) can be simplified in two distinct expressions according to whether the difference $N_1 - N_2$ is even or odd. In the case $N_1 - N_2 = 2k$, the ratio is

$$R^{(c)}_{{\rm ent},2k} = R^{(c)}_{\rm sep} + \frac{4L^{-2k}_{N_1}(q'^2)L^{2k}_{N_2}(q'^2)}{[L_{N_1}(q'^2) + L_{N_2}(q'^2)]^2}\cos(\Omega t). \tag{106}$$

It is seen that the $R^{(c)}_{{\rm ent},2k}$ oscillates around the $R^{(c)}_{\rm sep}$ with frequency Ω given by equation (105). If there is no detuning between the nonclassical electromagnetic fields, i.e. $\omega_1 = \omega_2$, then $R^{(c)}_{{\rm ent},2k}$ is constant, although it is still $R^{(c)}_{\rm ent} \neq R^{(c)}_{\rm sep}$. In the case $N_1 - N_2 = 2k + 1$ the ratio is

$$R^{(c)}_{{\rm ent},2k+1} = R^{(c)}_{\rm sep} - \frac{4L^{-2k-1}_{N_1}(q'^2)L^{2k+1}_{N_2}(q'^2)}{[L_{N_1}(q'^2) + L_{N_2}(q'^2)]^2}\frac{\cos(\Omega t)}{\tan(\omega_{\rm A}t)\tan(\omega_{\rm B}t)}. \tag{107}$$

In both cases the $R^{(c)}_{\rm ent}$ is time-dependent and it is a function of the photon frequencies ω_1, ω_2, in contrast to the case of $R^{(c)}_{\rm sep}$ (which is time-independent).

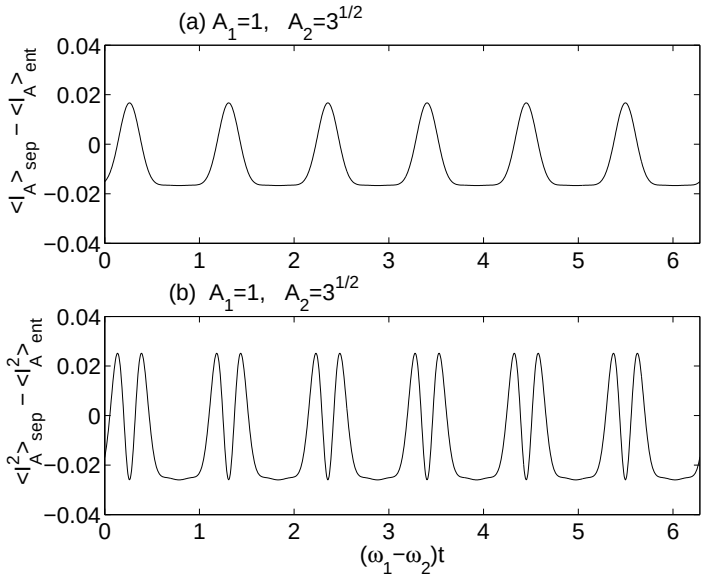

Figure 16. Difference of currents defined by equations (79) and (88) that are induced by separable and entangled photons in coherent states (for SQUID ring A). (a) $\langle I_{\rm A}\rangle_{\rm sep} - \langle I_{\rm A}\rangle_{\rm ent}$ and (b) $\langle I_{\rm A}^2\rangle_{\rm sep} - \langle I_{\rm A}^2\rangle_{\rm ent}$ corresponding to irradiation with separable and entangled coherent states of equations (22) and (24), for $A_1 = 1, A_2 = 3^{1/2}$ as a function of $(\omega_1 - \omega_2)t$, where $\omega_1 = 1.2 \times 10^{-4}$ and $\omega_2 = 10^{-4}$.

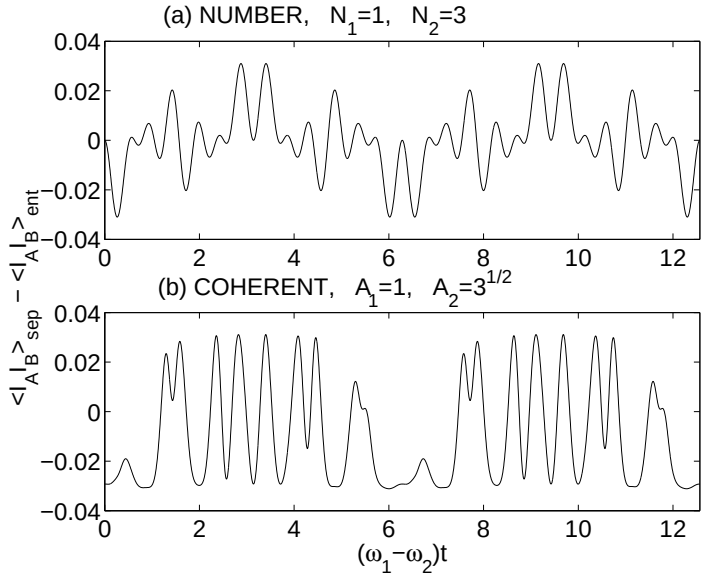

Figure 17. Difference of the product of currents $\langle I_{\rm A} I_{\rm B}\rangle_{\rm sep} - \langle I_{\rm A} I_{\rm B}\rangle_{\rm ent}$, defined by equation (85), that are induced by (a) the separable and entangled number states of equations (19), (20); and (b) the separable and entangled coherent states of equations (22), (24), for $N_1 = 1, N_2 = 3$ and $A_1 = 1, A_2 = 3^{1/2}$, respectively, as a function of $(\omega_1 - \omega_2)t$, where $\omega_1 = 1.2 \times 10^{-4}$ and $\omega_2 = 10^{-4}$.

8.5.2. Coherent states We consider the separable density operator $\rho_{\rm sep}$ of equation (22) and the entangled density operator $\rho_{\rm ent}$ of equation (24).

For the separable state of equation (22) the currents in A and B are

$$\langle \hat{I}_{\rm A}\rangle_{\rm sep} = \frac{I_1}{2}\exp(-\frac{q^{'2}}{2})\{\sin[\omega_{\rm A}t + 2q'|A_1|\cos(\omega_1 t - \theta_1)] + \sin[\omega_{\rm A}t + 2q'|A_2|\cos(\omega_1 t - \theta_2)]\}, \quad (108)$$

$$\langle \hat{I}_{\rm B}\rangle_{\rm sep} = \frac{I_2}{2}\exp(-\frac{q^{'2}}{2})\{\sin[\omega_{\rm B}t + 2q'|A_1|\cos(\omega_2 t - \theta_1)] + \sin[\omega_{\rm B}t + 2q'|A_2|\cos(\omega_2 t - \theta_2)]\}, \quad (109)$$

where $\theta_1 = \arg(A_1)$, and $\theta_2 = \arg(A_2)$. The expectation values of the product of the currents, and hence the ratios $R^{(c)}_{\rm sep}$ and $R^{(c2)}_{\rm sep}$, have been calculated numerically.

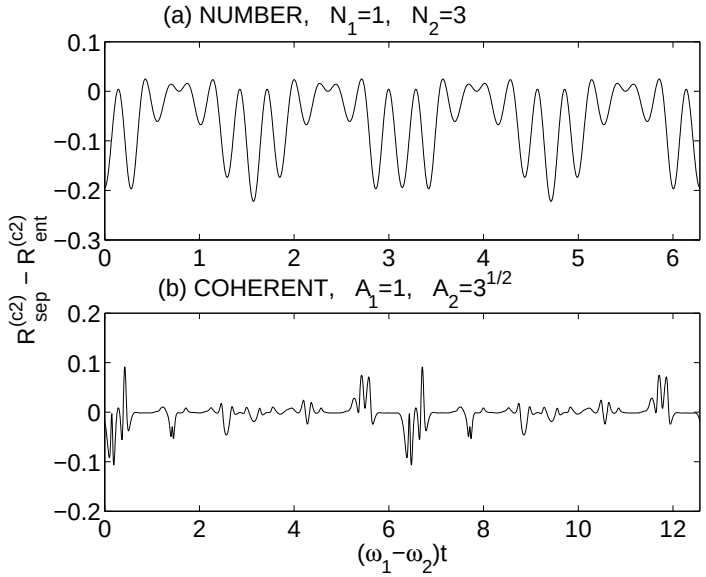

Figure 18. The difference $R^{(\rm c2)}_{\rm sep} - R^{(\rm c2)}_{\rm ent}$ corresponding to (a) the separable and entangled number states of equations (19), (20); and (b) the separable and entangled coherent states of equations (22), (24), for $N_1 = 1, N_2 = 3$ and $A_1 = 1, A_2 = 3^{1/2}$ as a function of $(\omega_1 - \omega_2)t$, where $\omega_1 = 1.2 \times 10^{-4}$ and $\omega_2 = 10^{-4}$.

For the entangled state of equation (24) the current in A is

$$\langle \hat{I}_{\rm A}\rangle_{\rm ent} = 2\mathcal{N}^2\langle \hat{I}_{\rm A}\rangle_{\rm sep} + \mathcal{N}^2 E F_1 \exp\left(-\frac{q^{'2}}{2}\right) I_1, \quad (110)$$

where

$$E = \exp[-|A_1|^2 - |A_2|^2 + 2|A_1 A_2|\cos(\theta_1 - \theta_2)], \quad (111)$$

and

$$F_1 = \{\exp[q|A_1|S_{A,1}(t) - q|A_2|S_{A,2}(t)] + \exp[-q'|A_1|S_{A,1}(t) + q'|A_2|S_{A,2}(t)]\} \times \sin[\omega_A t + q'|A_1|C_{A,1}(t) + q'|A_2|C_{A,2}(t)]. \quad (112)$$

The terms entering the factor F_1 are trigonometric functions of the form

$$\begin{aligned} S_{A,1} &= \sin(\omega_1 t - \theta_1), \qquad S_{A,2} = \sin(\omega_1 t - \theta_2), \\ C_{A,1} &= \cos(\omega_1 t - \theta_1), \qquad C_{A,2} = \cos(\omega_1 t - \theta_2). \end{aligned} \tag{113}$$

Similarly the current in SQUID ring B is

$$\langle \hat{I}_{\rm B} \rangle_{\rm ent} = 2\mathcal{N}^2 \langle \hat{I}_{\rm B} \rangle_{\rm sep} + \mathcal{N}^2 E F_2 \exp\left(-\frac{q'^2}{2}\right) I_2, \tag{114}$$

where

$$\begin{aligned} F_2 = &\{\exp[q|A_1|S_{B,1}(t) - q|A_2|S_{B,2}(t)] + \exp[-q'|A_1|S_{B,1}(t) + q'|A_2|S_{B,2}(t)]\} \\ &\times \sin[\omega_B t + q'|A_1|C_{B,1}(t) + q'|A_2|C_{B,2}(t)], \end{aligned} \tag{115}$$

and

$$\begin{aligned} S_{B,1} &= \sin(\omega_2 t - \theta_1), \qquad S_{B,2} = \sin(\omega_2 t - \theta_2), \\ C_{B,1} &= \cos(\omega_2 t - \theta_1), \qquad C_{B,2} = \cos(\omega_2 t - \theta_2). \end{aligned} \tag{116}$$

The expectation values of the product of the currents, and hence the ratios $R^{(c)}_{\rm ent}$ and $R^{(c2)}_{\rm ent}$, have been calculated numerically.

8.5.3. Numerical results In figures 14-18 we plot the results against dimensionless time $(\omega_1 - \omega_2)t$, where the photon frequencies are $\omega_1 = 1.2 \times 10^{-4}$ and $\omega_2 = 10^{-4}$. Other fixed parameters are the number of photons in the number states: $N_1 = 1, N_2 = 3$; and the average number of photons in the coherent states: $A_1 = 1, A_2 = 3^{1/2}$ (we take these values so that the microwaves in number and coherent states contain the same average number of photons).

In figure 14 we present the $R^{(\rm c)}_{\rm sep}$ for the separable number state of equation (19) (line of circles) and the $R^{(\rm c)}_{\rm sep}$ for the separable coherent state of equation (22) (solid line). It is seen that separable photons in different quantum states induce different correlations $R^{(\rm c)}$ between the Josephson currents in the distant SQUID rings.

In figure 15 we show the difference $R^{(\rm c)}_{\rm sep} - R^{(\rm c)}_{\rm ent}$ corresponding to (a) the separable and entangled number states of equations (19), (20); and (b) the separable and entangled coherent states of equations (22), (24). In this case the separable and entangled photons induce different correlations $R^{(\rm c)}$ between the Josephson currents.

In figure 16 we present (a) $\langle I_{\rm A} \rangle_{\rm sep} - \langle I_{\rm A} \rangle_{\rm ent}$ and (b) $\langle I^2_{\rm A} \rangle_{\rm sep} - \langle I^2_{\rm A} \rangle_{\rm ent}$ corresponding to irradiation with separable and entangled coherent states of equations (22) and (24).

In figure 17 we show the $\langle I_{\rm A} I_{\rm B} \rangle_{\rm sep} - \langle I_{\rm A} I_{\rm B} \rangle_{\rm ent}$ that are induced by (a) the separable and entangled number states of equations (19), (20); and (b) the separable and entangled coherent states of equations (22), (24).

In figure 18 we plot the difference $R^{(\rm c2)}_{\rm sep} - R^{(\rm c2)}_{\rm ent}$ corresponding to (a) the separable and entangled number states of equations (19), (20); and (b) the separable and entangled coherent states of equations (22), (24).

9. Discussion

We have studied electron interference in mesoscopic devices in the presence of nonclassical electromagnetic fields. The phase factor is in this case a quantum mechanical operator, whose expectation value with respect to the density matrix of the electromagnetic field determines the electron interference. We have presented various examples, which show that the quantum noise of the photons destroys slightly the electron interference fringes. Related is also the fact that the photon statistics affects the interfering electrons. These ideas have also been applied in the context of mesoscopic SQUID rings.

In certain cases we get novel quantum phenomena with no classical analogue. For example, in the case of a mesoscopic SQUID ring irradiated with microwaves in a squeezed vacuum state we get Shapiro steps only at even multiples of the fundamental frequency.

An important feature of nonclassical electromagnetic fields is entanglement. We have considered two distant mesoscopic electron interference devices that are irradiated with a two-mode nonclassical electromagnetic field. Each field mode is coupled to one of the mesoscopic devices. For entangled electromagnetic fields, the electric currents and their higher moments become correlated.

All our results have been derived within the external field approximation where the back reaction (additional flux created by the electrons) is negligible. This is a valid approximation in devices with small inductance.

Most of the experimental work on mesoscopic devices has studied their interaction with classical electromagnetic fields, until recently [24]. Our results show that there is merit in having a full quantum system where both the mesoscopic device and the electromagnetic field are quantum mechanical. In this case we can have purely quantum phenomena, without classical analogue, such as the entanglement of distant mesoscopic devices.

References

[1] Y. Aharonov and D. Bohm, Phys. Rev. **115**, 485 (1959)
W.H. Furry and N.F. Ramsey, Phys. Rev. **110**, 629 (1960)
S. Mandelstam, Ann. Phys. (N.Y.) **19**, 1 (1962)
T.T. Wu and C.N. Yang, Phys. Rev. D **12**, 3845 (1975)
S. Olariu and I. I. Popescu, Rev. Mod. Phys. **57**, 339 (1985)
M. Peshkin and A. Tonomura, *The Aharonov-Bohm Effect*, Lecture notes in Physics Vol. 340 (Berlin: Springer, 1989)

[2] S. Washburn and R.A. Webb, Adv. Phys. **35**, 375 (1986)
A.G. Aronov and Y.V. Sharvin, Rev. Mod. Phys. **59**, 755 (1987)
M. Pepper, Proc. Royal Soc. Lond. A **420**, 1 (1988)
G. Hackenbroich, Phys. Rep. **343**, 464 (2001)

[3] Y. Imry, *Introduction to Mesoscopic Physics* (NY: Oxford University Press, 1997)
S. Datta, *Electronic Transport in Mesoscopic Systems* (Cambridge: University Press, 1995)

D.K. Ferry and S.M. Goodnick, *Transport in Nanostructures* (Cambridge: University Press, 1997)

[4] U. Eckern and P. Schwab, J. Low Temp. Phys. **126**, 1291 (2002)

[5] M. Buttiker, A. Pretre, H. Thomas, Phys. Rev. Lett. **70**, 4114 (1993)
J.B. Pieper and J.C. Price, Phys. Rev. Lett. **72**, 3586 (1994)
J. Cohen, Y. Avishai, J. Phys. Cond. Matter **7**, 8791 (1995)

[6] M. Büttiker, Y. Imry, R. Landauer, Phys. Lett. A **96**, 365 (1983)
Y. Gefen, Y. Imry, M.Ya. Azbel, Phys. Rev. Lett. **52**, 129 (1984)
M. Buttiker, Y. Imry, M.Ya. Azbel, Phys. Rev. A **30**, 1982 (1984)

[7] L.P. Levy, G. Dolan, J. Dunsmuir, H. Bouchiat, Phys. Rev. Lett. **64**, 2074 (1990)
B. Reulet, H. Bouchait, D. Mailly, Europhys. Lett. 31, **305** (1995)
R. Deblock, Y. Noat, H. Bouchiat, B. Reulet, D. Mailly, Phys. Rev. Lett. **84**, 5379 (2000)
R. Deblock, R. Bel, B. Reulet, H. Bouchiat, D. Mailly, Phys. Rev. Lett. **89**, 206803 (2002)

[8] V. Chandrasekhar, R.A. Webb, M.J. Brady, M.B. Ketchen, W.J. Gallagher, A. Kleinsasser, Phys. Rev. Lett. **67**, 3578 (1991)

[9] A. Vourdas, Europhys. Lett. **32**, 289 (1995)
A. Vourdas, Phys. Rev. B **54**, 13175 (1996)
A. Vourdas and B.C. Sanders, Europhys. Lett. **43**, 659 (1998)
A. Vourdas, Contemp. Phys. **44**, 259 (2003)

[10] A. Vourdas, Phys. Rev. A **64**, 053814 (2001)
C.C. Chong, D.I. Tsomokos, A. Vourdas, Phys. Rev. A **66**, 033813 (2002)

[11] B. Lee, E. Yin, T.K. Gustafson, and R. Chiao, Phys. Rev. A **45**, 4319 (1992)

[12] L.H. Ford, Phys. Rev. D **47**, 5571 (1993)
F.D. Mazzitelli, J.P. Paz, and A. Villanueva, Phys. Rev. A **68**, 062106 (2003)
J.T. Hsiang and L.H. Ford, Phys. Rev. Lett. **92**, 250402 (2004)

[13] D. Mailly *et al.*, Phys. Rev. Lett. **70**, 2020 (1990)
B. Reulet, M. Ramin, H. Bouchiat, D. Mailly, Phys. Rev. Lett. **80**, 4955 (1998)

[14] M. Büttiker, J. Low Temp. Phys. **118**, 519 (2000)
M.V. Entin and M.M. Mahmoodian, J. Phys.: Condens. Matter **12**, 6845 (2000)
F. Marquardt and C. Bruder, Phys. Rev. B **65**, 125315 (2002)

[15] R. Loudon and P.L. Knight, J. Mod. Optics **34**, 709 (1987)
R. Loudon, *The Quantum Theory of Light* (Oxford: University Press, 2000)
D.F. Walls and G. Milburn, *Quantum Optics* (Springer, Berlin, 1994)

[16] B. Yurke, P.G. Kaminsky, R.E. Miller, E.A. Whittaker, A.D. Smith, A.H. Silver, R.W. Simon, Phys. Rev. Lett. **60**, 764 (1988)
B. Yurke, L.R. Corruccini, P.G. Kaminsky, L.W. Rupp, A.D. Smith, A.H. Silver, R.W. Simon, E.A. Whittaker, Phys. Rev. A **39**, 2519 (1989)
P. Bertet, S. Osnaghi, P. Milman, A. Auffeves, P. Maioli, M. Brune, J.M. Raimond, S. Haroche, Phys. Rev. Lett. **88**, 143601 (2002)
S. Haroche, Phil. Trans. R. Soc. Lond. A **361**, 1339 (2003)

[17] R.F. Werner, Phys. Rev. A **40**, 4277 (1989)
R. Horodecki and M. Horodecki, Phys. Rev. A **54**, 1838 (1996)
A. Peres, Phys. Rev. Lett. **77**, 1413 (1996)
V. Vedral, M.B. Plenio, M.A. Rippin, P.L. Knight, Phys. Rev. Lett. **78**, 2275 (1997)
V. Vedral, Rev. Mod. Phys. **74**, 197 (2002)

[18] A. Aspect, P. Grangier, and G. Roger, Phys. Rev. Lett. **47**, 460 (1981)
J.M. Raimond, M. Brune, S. Haroche, Rev. Mod. Phys. **73**, 565 (2001)
G.D. Giuseppe, M. Atatüre, M.D. Shaw, A.V. Sergienko, B.E.A. Saleh, M.C. Teich, Phys. Rev. A **66**, 013801 (2002)

[19] D.I. Tsomokos, C.C. Chong, and A. Vourdas, Phys. Rev. A **69**, 013810 (2004)
D.I. Tsomokos, New J. Phys. **7**, 50 (2005)

[20] B.D. Josephson, Rev. Mod. Phys. **36**, 216 (1964)
S. Shapiro, A.R. Janus, and S. Holly, Rev. Mod. Phys. **36**, 223 (1964)
B.D. Josephson, Adv. Phys. **14**, 419 (1965)
[21] N. Byers and C.N. Yang, Phys. Rev. Lett. **7**, 46 (1961)
F. Bloch, Phys. Rev. B **2**, 109 (1970)
A. Barone and G. Paterno, *Physics and Applications of the Josephson Effect* (NY: Wiley, 1982)
M. Tinkham, *Introduction to Superconductivity* (NY: McGraw-Hill, 1996).
[22] G. Schön and A.D. Zaikin, Phys. Rep. **198**, 237 (1990)
M.A. Kastner, Rev. Mod. Phys. **64**, 849 (1992)
Y. Makhlin, G. Schön, and A. Shnirman, Rev. Mod. Phys. **73**, 357 (2001)
[23] I. Chiorescu, Y. Nakamura, C. Harmans, J.E. Mooij, Science **299**, 1869 (2003)
Y. Nakamura, Y.A. Pashkin, J.S. Tsai, Nature **398**, 786 (1999)
C.H. van der Wal, A.C.J. ter Haar, F.K. Wilhem, R.N. Schouten, C.J.P.M. Harmans, T.P. Orlando, S. Lloyd, J.E. Mooij, Science **290**, 773 (2000)
D. Vion, A. Aassime, A. Cottet, P. Joyez, H. Pothier, C. Urbina, D. Esteve, and M.H. Devoret, Science **296**, 886 (2002).
[24] A. Wallraff, D.I. Schuster, A. Blais, L. Frunzio, R.S. Huang, J. Majer, S. Kumar, S.M. Girvin, and R.J. Schoelkopf, Nature **431**, 162 (2004)
A. Blais, R.S. Huang, A. Wallraff, S.M. Girvin, and R.J. Schoelkopf, Phys. Rev. A **69**, 062320 (2004)
[25] A. Vourdas, Phys. Rev. B **49**, 12040 (1994)
[26] A. Vourdas, Z. Phys. B **100**, 455 (1996)
[27] A. Vourdas and T.P. Spiller, Z. Physik B **102**, 43 (1997)
M.J. Everitt, P. Stiffell, T.D. Clark, A. Vourdas, J.F. Ralph, H. Prance, R.J. Prance, Phys. Rev. B **63**, 144 530 (2001)
[28] A.A. Odintsov and A. Vourdas, Europhys. Lett. **34**, 385 (1996)
L.M. Kuang, Y. Wang, and M.L. Ge, Phys. Rev. B **53**, 11 764 (1996)
J. Zou, B. Shao, and X.S. Xing, Phys. Rev. B **56**, 14 116 (1997)
W. Al-Saidi and D. Stroud, Phys. Rev. B **65**, 014512 (2002)
[29] D.I. Tsomokos, C.C. Chong, and A. Vourdas, J. Phys.: Condens. Matter **16**, 9169 (2004)
A. Vourdas, D.I. Tsomokos, and C.C. Chong, quant-ph/0406059 (2004)
[30] M. Paternostro, G. Falci, M. Kim, and G.M. Palma, Phys. Rev. B **69**, 214502 (2004)
Z. Kis and E. Paspalakis, Phys. Rev. B **69**, 024510 (2004)
[31] C. Bena, S. Vishveshwara, L. Balents, and M.P.A. Fisher, Phys. Rev. Lett. **89**, 037901 (2002)
N.M. Chtchelkatchev, G. Blatter, G.B. Lesovik, and T. Martin, Phys. Rev. B **66**, 161320 (2002)
A. Crepieux, R. Guyon, P. Devillard, and T. Martin, Phys. Rev. B **67**, 205408 (2003)
M. Buttiker, P. Samuelsson, and E.V. Sukhorukov, Physica E **20**, 33 (2003)
P. Samuelsson, E.V. Sukhorukov, and M. Buttiker, Phys. Rev. Lett. **92**, 026805 (2004)
A.V. Lebedev, G. Blatter, C.W.J. Beenakker, and G.B. Lesovik, Phys. Rev. B **69**, 235312 (2004)
L. Faoro, F. Taddei, and R. Fazio, Phys. Rev. B **69**, 125326 (2004)
[32] N.L. Balazs and B.K. Jennings, Phys. Rep. **104**, 347 (1984)
M. Hillery, R.F. O' Connell, M.O. Scully, and E.P. Wigner, Phys. Rep. **106**, 121 (1984)
H.W. Lee, Phys. Rep. **259**, 147 (1995)
V. Buzek and P.L. Knight, Prog. Opt. **34**, 1 (1995)
[33] S.M. Roy and V. Singh, Phys. Rev. D **25**, 3413 (1982)
[34] I. S. Gradshteyn and I. M. Ryzhik, *Table of Integrals, Series, and Products*, 6^{th} ed. (2000) Academic Press
[35] L. Mandel and E. Wolf, *Optical Coherence and Quantum Optics* (Cambridge: University Press, 1995)